OVERVIEW OF ODS ALLOY DEVELOPMENT

Ian Wright, Bruce Pint, and Zhao Ping Lu
Metals & Ceramics Division, ORNL, 1 Bethel Valley Road, Oak Ridge, TN 37831
E-mail: wrightig@ornl.gov; telephone: 865.574.4451; fax: 865.241.0215

ABSTRACT

The overall goal of this effort is to address the materials-related barriers to expediting the use of oxide dispersion-strengthened (ODS) alloys in components required in the U.S. Department of Energy's (DOE's) Office of Fossil Energy's advanced coal combustion, gasification, and utilization processes to operate at temperatures higher than are possible with conventionally-strengthened alloys. The project is focused on the needs of the broad range of ferritic ODS-alloys, especially the FeCrAl-based alloys, with the purpose of developing a detailed understanding of the behavior of ODS alloys in all phases of their use, including fabrication, service performance, life prediction, mode of failure, repair, and refurbishment. The intended output of this project is a compilation of information that facilitates the assessment of the applicability of ODS alloys to the needs of high-temperature equipment required in DOE's advanced power plants.

Particular emphasis has been placed on processing modifications to increase the hoop strength of ODS tubes, on joining, and on oxidation-limited life prediction. Approaches for modifying the alloy grain structure to increase the creep strength in the transverse/hoop direction (for tubes) have involved the examination of processes that modify the secondary recrystallization behavior of the alloy, with the intention of producing larger, more equiaxed grains, or a spiral grain structure that reduces the number of transverse grain boundaries. Processing using a commercial-scale pilgering/flow-forming/cross-rolling facility indicated the potential of this route, but also revealed some practical difficulties, especially since such processing of ODS alloys must be done at temperatures above approximately 600°C. Research to provide guidance for such processing has involved measurements using well-controlled, hot torsion testing, as well as trials with a small-scale cross-rolling mill. Progress has been made with joining approaches that involve inertia welding, and diffusion bonding, and the creep strength of butt joints made by some of the process variations approaches the transverse creep strength of the parent alloy.

A particular feature of the ferritic ODS-FeCrAl alloys is that they exhibit relatively low oxidation rates up to 1200°C (2192°F), due to the formation of a protective Al_2O_3 film. In service, the mechanical load applied to these ODS alloys will be below the stress level at which significant creep occurs, so that it is likely that the effective service lifetime will be determined by the rate of environmental degradation. Operation at the very high temperatures possible with these alloys means that, should the ability to form a protective oxide scale be lost, the ensuing oxidation damage could be very rapid. However, since during protective oxidation there is very little loss in alloy section due to the thin alumina scales formed, it is doubtful that mechanical means for monitoring the rate consumption of the alloy would provide sufficient accuracy for assessment of remaining lifetime. Hence, there is a need for some form of lifetime model to provide reliable prediction of remaining lifetime in typical service environments. Efforts to develop a lifetime model are in progress for the condition where the life-limiting process is oxidation in air (or oxygen); some data also have been generated in reducing environments (where there is potential for sulfidation attack); and in steam. Comparison of predictions from the model with results from lifetime testing in air indicate that good progress is being made.

INTRODUCTION

The goal of this project is to facilitate the exploitation of ODS alloys. There are several perceived barriers to the practical use of these alloys, the most prominent of which are (1) the fact that the alloys cannot be satisfactorily joined by conventional fusion techniques, and (2) the alloys are expensive because they are made by a power metallurgy route. Further, they have some unusual mechanical traits, in that they have highly-directional properties such that in tube form, the creep strength in the transverse or hoop direction usually is only approximately 50% of that in the axial direction. For joining, provided that the effects on the alloy microstructure (hence its mechanical properties) are understood, there are several unconventional techniques that can be applied. Any approach to increase the transverse creep strength of ODS alloy tubes requires the ability to modify the recrystallized grain structure of the alloy. Various innovative processing routes are being explored with the aim of promoting the formation of large, equiaxed (as opposed to the usual long, thin, high aspect ratio) grains, or the realignment of the grains to present fewer grain boundaries aligned normal to the hoop stress direction. Other activities are intended to provide better quantification of the alloy properties and its characteristic behavior to ensure that there are no surprises in the practical application of these alloys, and to provide a database of properties required by designers.

The focus on ODS alloys results because of their exceptional creep strength at high temperatures. The advantages of ODS alloys over conventional wrought or cast Ni-Fe-Cr alloys are shown schematically in Fig. 1, which plots the average 100,000 hour stress rupture strength for all wrought and cast high temperature alloys as a function of temperature [1]. Also in Fig. 1 is shown the theoretical maximum 100,000 hour stress rupture strength for these alloys, calculated on the assumption that the strengthening phases used in these alloys are able to attain their maximum theoretical stability in practice. Note that the difference between the two trend lines (at 950°C, for instance) is significant and, in fact, represents the potential for further development of these conventional alloys. The trend line for available ODS-FeCrAl ferritic alloys (extrapolated from 10,000-h data) suggests that they already possess creep strength that exceeds the maximum potential strength of conventional alloys (a factor of 3-4 times at 950°C in the axial

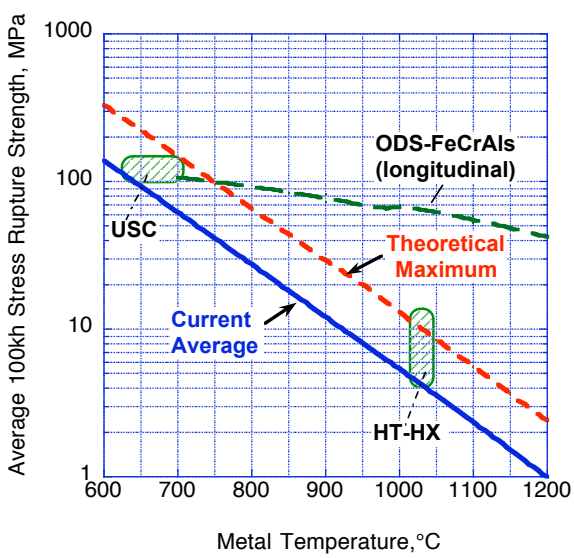

Figure 1. Comparison of the Temperature–Dependence of Actual and Theoretical Creep-Rupture Strength of Wrought or Cast Ni-Fe-Cr Alloys as a Function of Temperature.

direction), and this advantage is even greater at higher temperatures. Such properties provide the potential for using metallic materials at temperatures where typically ceramics have to be considered. However, it is noted that the stress rupture strength of these ODS alloys in the transverse direction is much lower than the axial strength, as discussed earlier. A further advantage of these ODS FeCrAl alloys is that they have excellent high-temperature oxidation resistance, and good resistance to sulfidation and to steam oxidation.

The initial phase of this project was aimed at the development of an ODS-version of Fe_3Al, which has been shown to possess excellent resistance to high-temperature oxidation, and especially to have resistance to sulfidation that is significantly greater than the commercial ODS-FeCrAl alloys [2]. This objective was achieved, with the resulting ODS-Fe_3Al alloy exhibiting equivalent creep strength to commercial alloy MA956, as indicated in Fig. 2. With improved recrystallization processing, the creep-rupture strength of ODS-Fe_3Al, in fact, exceeds that of MA956 [3].

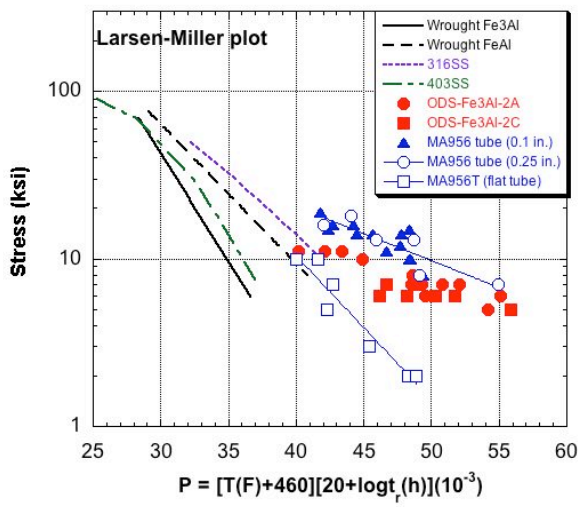

Figure 2. Summary of Creep Rupture Strength of ODS-Fe_3Al Alloys (PMWY-2A and -2C) Compared to MA956, and Selected Wrought Alloys.

The approach being followed in the current phase of this project has three main goals: (1) to understand and quantify all the available routes for joining all ODS-FeCrAl alloys, including ODS-Fe_3Al; (2) to develop mechanistic understanding of how to control the alloy microstructure, and so to tailor the properties depending on the form of alloy required for use; and (3) to develop a mathematical model of the oxidation behavior of these alloys to allow lifetime predictions, and to account for the effects of different environments. The compositions of the alloys of interest are listed in Table I.

Table I. Nominal Compositions of Ferritic ODS Alloys of Interest (weight percent).

Alloy	Fe	Cr	Al	Mo	W	Ti	Si	RE*
Kanthal APM	Bal	20.0	5.5	—	—	0.03	0.23	ZrO_2-Al_2O_3
INCO MA 956	Bal	20.0	4.5	—	—	0.5	—	Y_2O_3-Al_2O_3
INCO MA956HT	Bal	21.6	5.9	—	—	0.4	0.07	Y_2O_3-Al_2O_3
PM2000	Bal	20.0	5.5	—	—	0.5	—	Y_2O_3-Al_2O_3
Dour Alloy ODM 751	Bal	16.5	4.5	1.5	—	0.6	—	Y_2O_3-Al_2O_3
ODS-Fe_3Al	Bal	2.2	15.9	—	—	0.07	0.1	Y_2O_3-Al_2O_3

*reactive element addition, in the form of an oxide dispersion

INCREASED HOOP STRENGTH IN TUBES

Figure 3 summarizes the measured values (100-h incrementally-loaded creep tests) of the axial and transverse creep strength of tubes of alloy MA956, as a function of Larson-Miller parameters; the transverse (hoop) creep strength is approximately 35% of the axial creep strength. For tube applications, creep strength in the hoop direction is a critical parameter so that, if the promise of ODS alloys (as tubes)

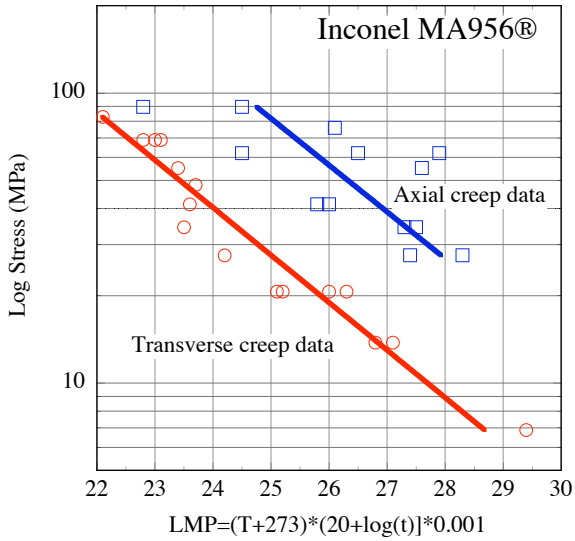

Figure 3. Summary of Failure Stresses in Creep in the Axial and Transverse Directions of Specimens taken From Tubes of Alloy MA956 (100-h incrementally-loaded tests).

is to be realized, it is important that the hoop creep strength be increased to the level attainable in the axial direction. Significant effort has been expended in previous programs in attempts to modify the recrystallization behavior of ferritic ODS alloys to change the shape of the recrystallized grains to attain this goal. The most cited example of significant progress in this direction is that of the "pancake" or "onion skin" grain structures achieved in the Dour Metal alloy ODM751 [4]; unfortunately, that company no longer exists, and the key personnel that developed the processing structures for this alloy have been dispersed and cannot be found. Attempts to reconstruct the suspected processing innovations used by Dour Metal, from personnel who collaborated in the production of ODM751 tubing for the COST 501 program, suggest that the main differences from standard ODS alloy processing occurred in the powder milling and pre-consolidation steps. In particular, it appears that a small addition of relatively large oxide particles was made towards the end of powder milling (apparently intended to act as nucleation sites during secondary recrystallization); the milled powder was pre-compacted using cyclic compaction (a process somewhat similar to cyclic channel deformation); and, before recrystallization, a small amount of cold work was imparted to the extruded tubes (as part of a tube-straightening process).

Although processing by Dour Metal [4] showed the possibility of producing an overlapping, 'onion skin'-type structure, as shown in Fig. 4, it has not been possible to date to reproduce this microstructure in current ODS FeCrAl alloys. While conventional approaches for modifying the alloy microstructure to produce a more equiaxed grain structure have met with little success, it appears that the flow-forming approach holds good promise, as shown by the results of initial trials on 8.9 cm OD, tubes of MA956 (Special Metals Corporation; trials at Dynamic Machine Works, Billerica, Massachusetts). Figure 5

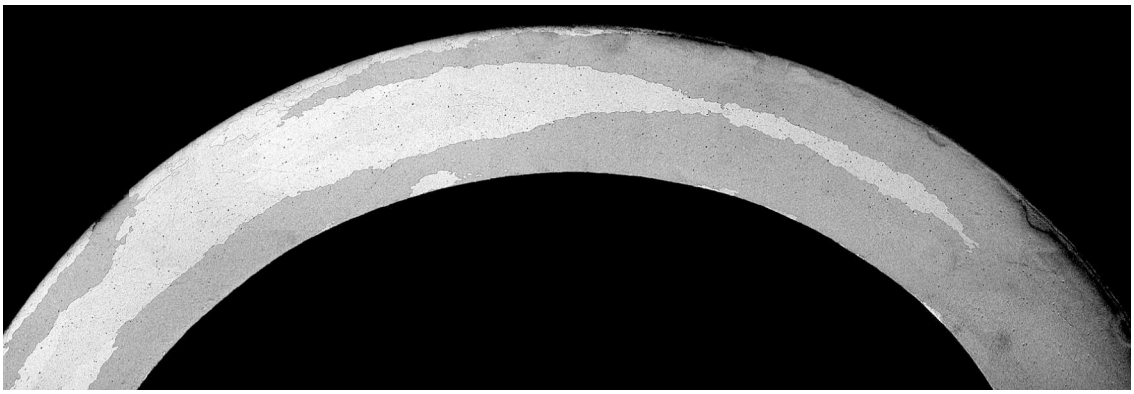

(a) Transverse cross section

(b) Longitudinal cross section

Figure 4. Microstructure of a 25 mm diameter, 2.5 mm wall tube of Dour Metal Alloy ODM751, showing the large, overlapping grains structure. In the longitudinal section shown in (b), the structure appears to consist of essentially two grains.

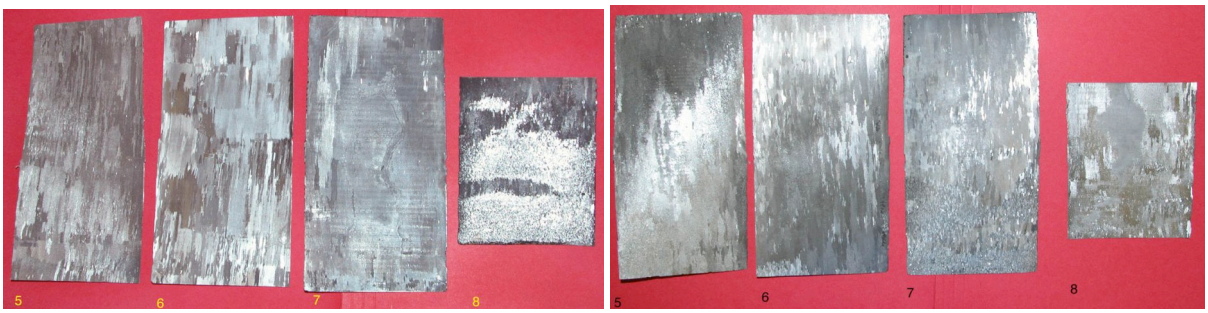

Figure 5. Grain Size of Specimens Taken From a Tube of Alloy MA956 After a Reduction in Wall Thickness of 80% by Flow-Forming.

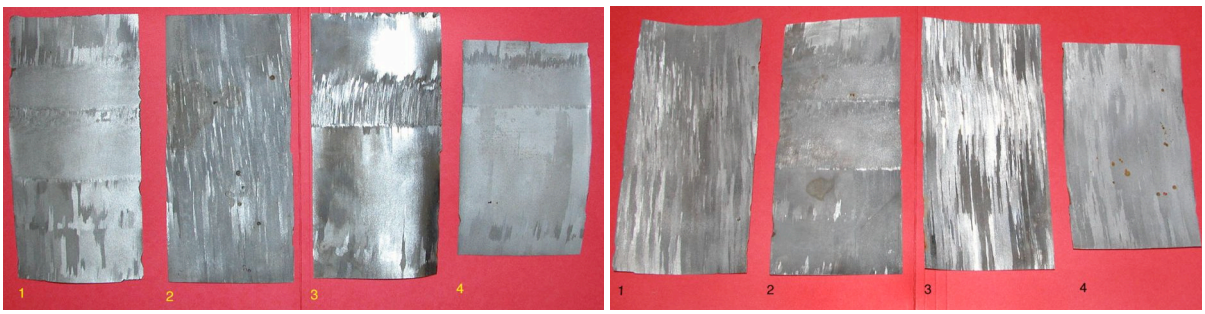

Figure 6. Grain Size of Specimens Taken From a Tube of Alloy MA956 After a Reduction in Wall Thickness of 90% by Flow-Forming.

shows the macro grain structure after 80% reduction of the tube wall thickness by flow forming; the tube was slit and flattened (by rolling between two plates at 800°C) after processing. Figure 6 shows similar microstructures after 90% reduction by flow forming. Although the tubes before flow forming had undergone secondary recrystallization, some further recrystallization was accomplished by heat treating for 6 hours at 1200°C. Comparison of the macro-grain structures on each side of the various specimens of flattened, flow-formed tubing indicates that significant changes in grain structure were achieved, but that the new grain structure was not uniform in size or shape, and consisted of discontinuous patches of similarly-shaped grains. The non-uniform microstructures probably resulted from the discontinuous nature of the processing in this initial trial, but certainly illustrate the potential for structural modification.

Figure 7 compares axial and transverse creep measurements made on specimens from these flattened tubes with the data shown earlier in Fig. 3 for the bulk alloy. While the results for transverse strength of the flow-formed tubes did not show the hoped-for trend to higher creep rupture strength compared to the bulk alloy, in one or two cases (for specimens that exhibited a large grain size in the transverse direction, shown in Fig. 8), somewhat higher creep strengths were measured. A possible reason for the mixed results from these tests was the difficulty of extracting creep specimens that had a consistent grain structure from the flow-formed tubes.

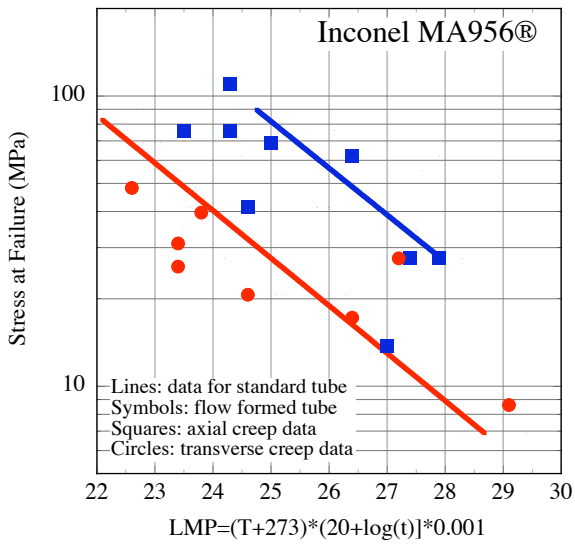

Figure 7. Summary of Failure Stresses in Creep in the Axial and Transverse Directions of Specimens taken From Flow-Formed Tubes of Alloy MA956 (100-h incrementally-loaded tests).

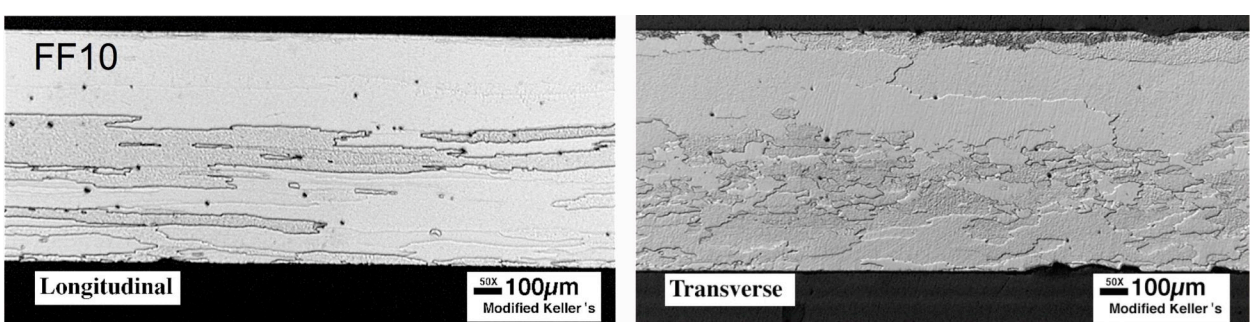

(a) Cross section after 80% reduction

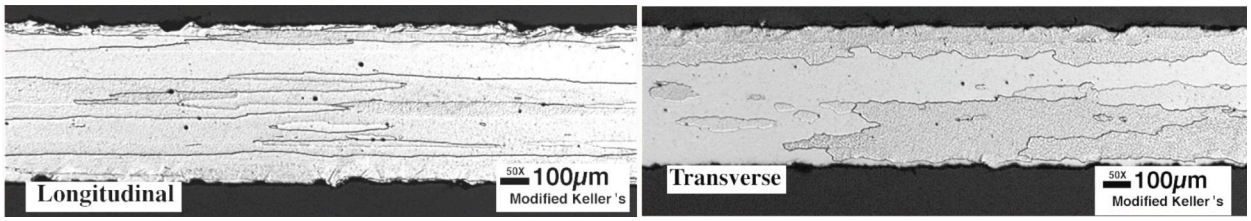

(b) Cross section after 90% reduction

Figure 8. Cross Sections of Flow-Formed MA956 Tube Showing the Alloy Microstructure.

In order to provide some guidance for the parameters to be used in future flow-forming trials, measurements of the torsional properties of these alloys as a function of temperature are being made, and these are being used in the planning of further forming trials aimed at exploring flow forming, ring-rolling, and forming under torsion.

JOINING OF ODS ALLOYS

The overall goal of this effort is to develop a database of containing descriptions of the practical aspects of available joining processes, together with quantitative data (preferably creep strength) and information on the effects of the joining processes on the alloy microstructure. Also to be included is quantification of any effects of the joints on the high-temperature oxidation behavior of the alloys. It is anticipated that the availability of such a database will encourage wider consideration of the use of ODS alloys.
The starting point for selecting joining techniques for ODS alloys is that any such process must avoid redistribution of the dispersed oxide phase, and must not unduly change a grain size, grain shape, or grain orientation in the alloy. These restrictions obviously present challenges, and indicate that conventional fusion joining processes probably are a last resort for these alloys. Earlier efforts have examined the application of friction welding [5] and inertia welding [6] to ODS alloys, and in both cases significant (and possibly unacceptable) distortion of the alloy microstructure resulted. Nevertheless, analysis of the joints produced suggested routes for minimizing the undesirable effects, so that efforts are continuing to revise the joining parameters.

Diffusion bonding was successfully applied to a chromium oxide-forming ODS alloy (Inconel MA754) in the construction of a serpentine heat exchanger in the US-DOE's HiPPS Program [7], and brazing using Pd-Ni braised with an alumina scale-forming alloy (PM2000) were investigated in a European COST-522 Program [8]. Further, a harp-design heat exchanger was successfully assembled from an alumina scale-forming ODS alloy (ODM 751) by explosively bonding the ODS alloy to safe ends made of thicker wall, high temperature NiCr alloy [9]. This heat exchanger was successfully demonstrated at metal temperatures in excess of 1,000°C. The technique of pulsed magnetic welding has been attempted in earlier programs for ODS-Fe-Cr alloys [10] and, since the joint produced has a structure that resembles that resulting from explosive bonding, this technique has continuing promise, provided that it can be applied to a sufficient range of product forms. In addition, whereas many of the joining trials have addressed butt joints in tubes, the potential for using different joint configurations that have the potential for using locally-thicker sections to compensate for any loss of strength in the joint, appear to have good potential for specific applications, and deserve further examination. In this program, the joining techniques considered include: inertia welding [6]; transient liquid-phase bonding; plasma-assisted diffusion bonding; and pulsed magnetic welding [6].

INERTIA WELDING

Inertia welding has been used to make butt joints in 6 cm OD x 5 mm wall, unrecrystallized MA956 tubes, as indicated schematically in Fig. 9. As anticipated, there was massive deformation of the alloy microstructure in the immediate vicinity of the joint (Fig. 10). However, this deformation was very localized, with a sharp demarcation visible with the original alloy microstructure (shown after recrystallization of the joined alloy), which clearly indicated that the large grains follow the axial direction of the tube to the boundary with the deformed material, at which point they follow the flow path of the deformed material in the joint. Because of the variation in alloy microstructure through the wall thickness of the alloy in the vicinity of the joint, the mechanical properties of the joint (in creep) are expected to vary with location through the joint. Creep testing of specimens extracted from locations where obvious differences in microstructure prevailed is in progress. Note also that the joining parameters used were far from being optimized for this alloy; the results of these analyses will be used to iterate those parameters in search of maximum joint creep strength.

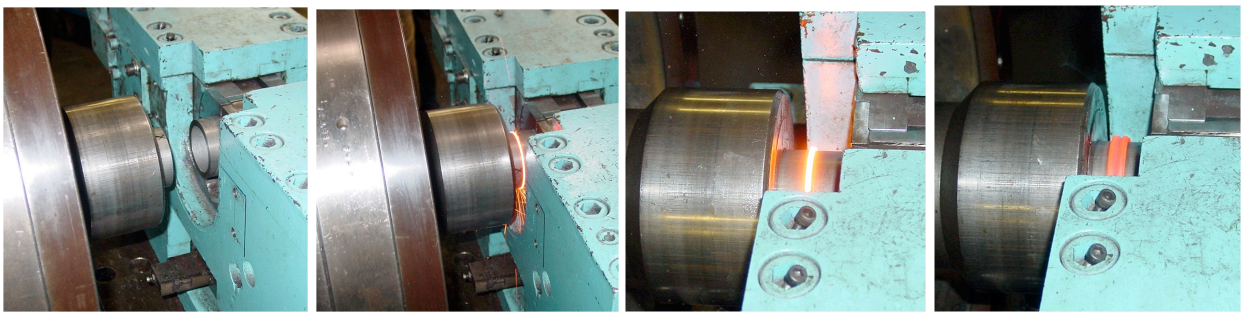

(a) Spin-up (b) Initial contact (c) Flywheel stopped (d) Cool down

(e) As-joined tube

Figure 9. Sequences in the Inertia Welding of a MA956 Tube.

TRANSIENT LIQUID-PHASE BONDING

The transient liquid-phase (TLP) bonding approach being used builds on a technique that was used successfully in the HiPPS program [7]. In that program, a nickel-based brazing alloy [Ni-9.5Cr-3Al-4.9Ti-7(Mo+W)-4.5Si-0.7B, weight percent] was used to join tubes of a chromia scale-forming ODS Ni-20Cr-Ti alloy to corner blocks made of the same material, in the construction of a serpentine heat exchanger. That heat exchanger performed exceptionally well in coal fired trials [12]. Examination of the

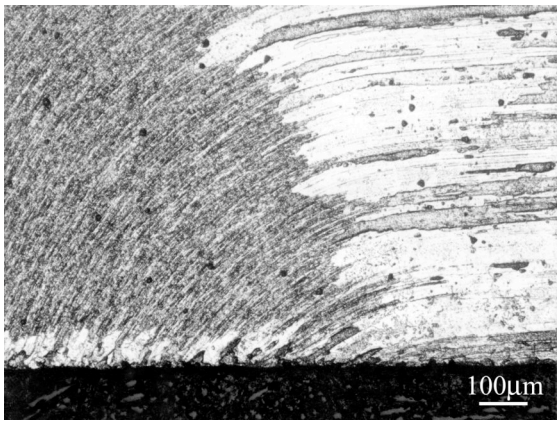

Figure 10. Cross Section of the Joint formed in MA956 by Inertia Welding, Showing the Extent of Microstructural Deformation.

joints suggested that they were by no means optimum, partly due to differences in the extent of diffusion of the brazing alloy away from the joint, resulting from the fact that the alloy grain size in the ODS tubes and corner blocks ranged from coarse-grained (in the tubes) to very fine-grained (blocks).

Figure 11 shows a schematic representation of such joints, while Fig. 12 shows the microstructure of one such joint and, in particular, the obvious differences in the depth of diffusion of the brazing alloy away from the joint in the two materials as a result of the large difference in the numbers of diffusion paths resulting from the different alloy grain sizes. There was an indication of some redistribution of the Y content of the ODS alloy as YAG particles, particularly in the coarse-grained tube. There was also a line

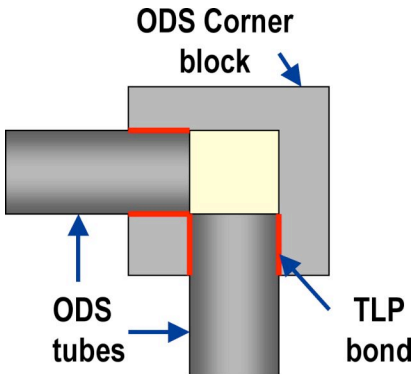

Figure 11. Cross Section of a Tube-to-Corner Block Joint Made by TLP Bonding in Ni-based ODS Alloy Inconel MA754 (Ni-20Cr-1Ti-0.5Y_2O_3)

of voids approximately 150 μm from the joint (Fig. 12a), but only on the large-grained tube side. These microstructural changes have obvious implications for reduction of the creep strength in any joint, but inthe joint configuration used these were not important, because of the particularly thick cross sections employed.

The considerations used in developing this joining technique have been used to modify the parameters to develop a TLP bonding alloy suitable for application to an ODS FeCrAl alloy, for which joining is more problematic because of its ability to form a tenacious aluminum oxide film. In principle, the TLP technique involves placing a thin film (initially, in this case, foil) of the TLP alloy along the interface to

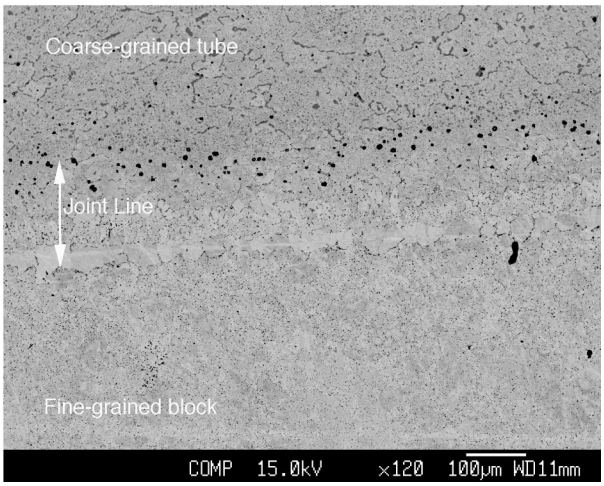

(a) Secondary Electron Image (coarse-grained tube is above the joint; fine-grained is block below)

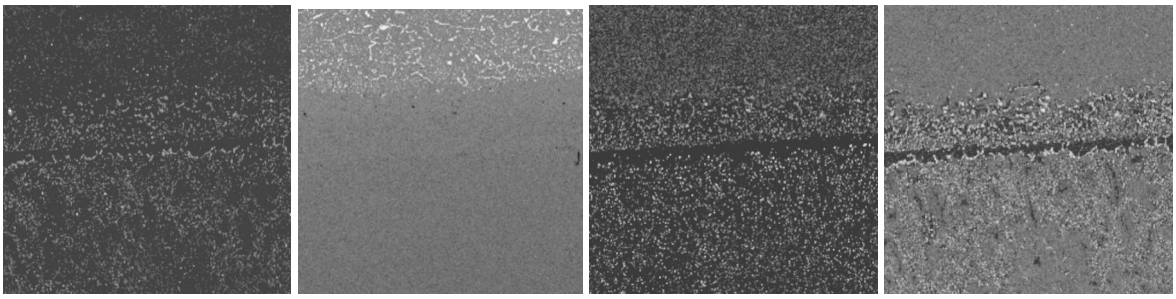

(b) Al (c) Cr (d) Ti (e) Y

Figure 12. Cross Section of Joint Made in Nickel-Based ODS Alloy MA754 by TLP Bonding, Showing the Overall Appearance of the Joint, and the Distribution of Al, Cr, Ti, and Y.

be joined; applying pressure to the joint; and heating it to a temperature at which the TLP alloy melts. This is followed by holding at a temperature for sufficient time for interdiffusion to occur across the joint, then a further hold at a temperature sufficient for the TLP constituents to diffuse away from the bond line, and to disperse in the host alloy. Figure 13 shows microstructures across such joints made by TLP bonding of segments of a 6 cm OD, 5 mm wall tube of alloy MA956, following joining treatments at three different temperatures. (Note that, in this case, the less-desirable, large-grained form of the alloy

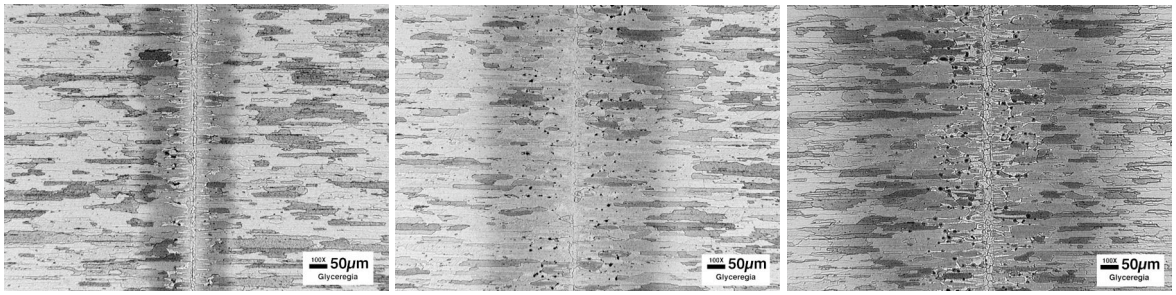

(a) 900°C (b) 1080°C (c) 1180°C

Figure 13. Cross Section of Joints Made in Alloy MA956 by TLP Bonding (showing effects of increased temperature on the post-joining diffusion treatment).

was used, because of the unavailability of fine-grained, unrecrystallized material). While the micro-appearance of the joints indicated that they were relatively clean, it was obvious that a line of voids (displaced on either side of the joint) was present, and that these became more numerous or larger with increasing processing temperature. Figure 14 illustrates obvious displacement of the alloy microstructure

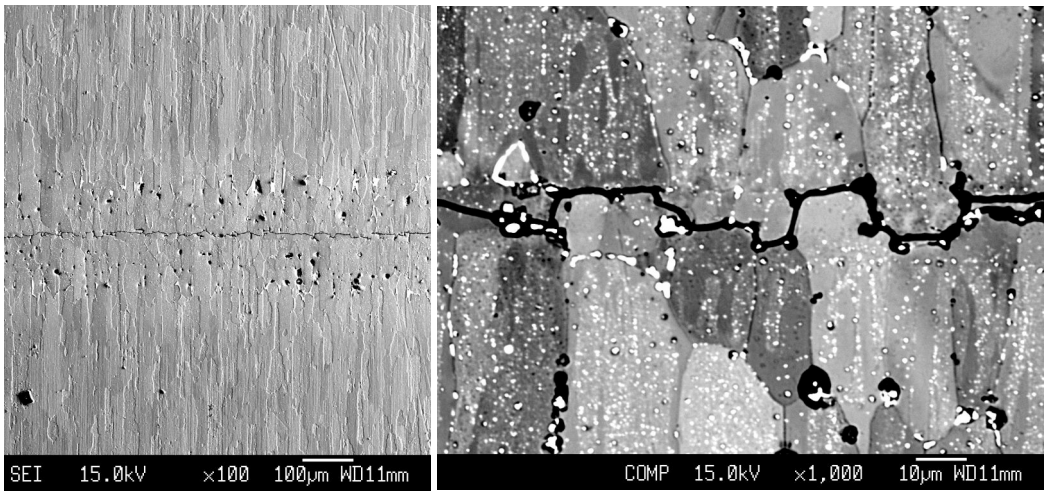

(a) Secondary electron image (b) Backscattered image, showing distribution of elements from the TLP alloy

Figure 14. Details of TLP Bonded Joint in MA956, showing Micro-Displacement of the Joint Interface.

that occurred across the bond line, as well as the fact that one of the components of the TLP alloy was present in the vicinity of the joint as discrete precipitates along alloy grain boundaries and subgrain boundaries (bright-appearing phase), with larger precipitates at some grain boundaries. These results suggest that different phases from those expected from thermodynamic calculations may have been formed and, as a result, those calculations are being revised. In fact, those joints were found to have very little strength when tested in tension (stress axis perpendicular to the joint).

Oxidation exposures at 1250°C in air (100-hour cycles) indicated an increased tendency for scale spallation from these samples, as shown in Fig. 15. However, detailed post-test examination showed that the increased scale spallation was not focused on the joint areas; presumably, the observed difference reflected a slight difference in behavior between the alloy used for the joints, and that used in generating the baseline oxidation kinetics. There was no indication of faster oxide growth at or near the bond line, in contrast to that reported for other joining techniques [13].

PLASMA-ASSISTED DIFFUSION BONDING

Plasma-assisted diffusion bonding, which is being developed by MER Corporation, in Tucson, Arizona, has shown excellent promise in producing clean-appearing butt joints in alloy MA956. This process was derived from the plasma-assisted sintering processing used for consolidating ceramic powders, in which micro plasma discharges occur between separate particles in the powder and facilitate consolidation. In joining, a direct electric current is applied to the interface to be joined, while pressure is applied to the joint. It is thought that micro plasma discharges occur at the interface, essentially cleaning off the inherent alumina film formed on MA956, so facilitating mass transfer and bonding.

Iteration of the initially-selected parameters resulted in joints which exhibited creep strength (stress axis perpendicular to the joint) that compared favorably with the transverse creep strength measured for

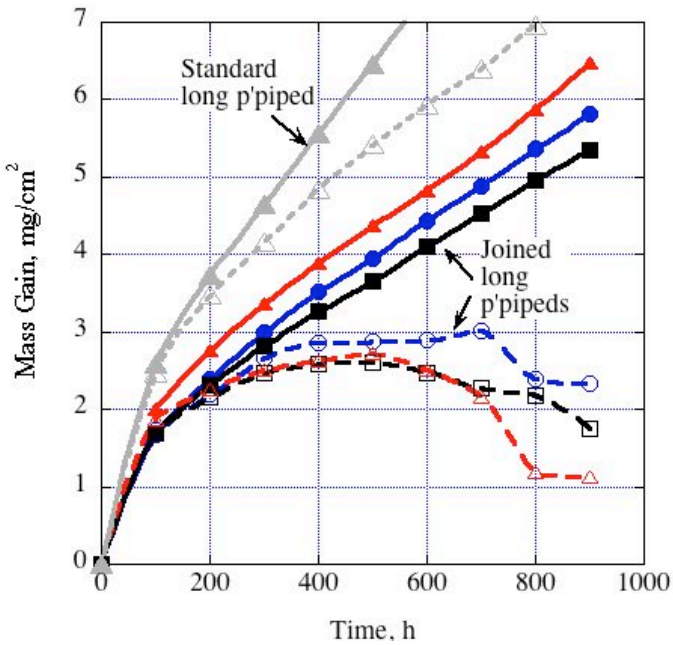

Figure 15. Comparison of Oxidation Kinetics for TLP-Bonded Alloy 956 With Those For Bulk Alloy (1250°C, 100-h cycles in air; solid lines represent the total mass gain, whereas dashed lines represent the specimen mass change).

specimens taken from flattened tubing, Fig. 16. Note that in this figure the range of axial creep data is for specimens from tubes of different diameters (and different alloy grain sizes); however, the data points for two bulk (non-joined) reference specimens from the batch of material used in the joining tests agree very

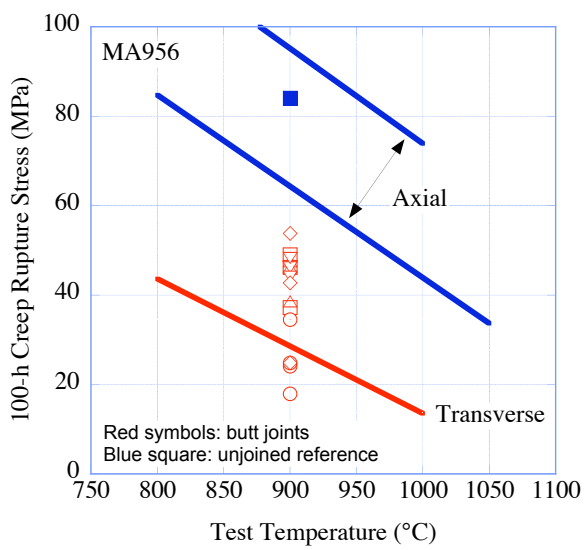

Figure 16. Comparison of Creep Strength of Plasma-Assisted Diffusion Bonding of MA956 to Itself, with that of the Bulk Alloy.

well with these reference data. Figures 17 and 18 show a metallographic cross section of such a joint, and details of the precipitates found along it. These indicate that the revised processing procedure resulted in a significant reduction in the population of particles (TiC and Al_2O_3) and voids that were found to decorate

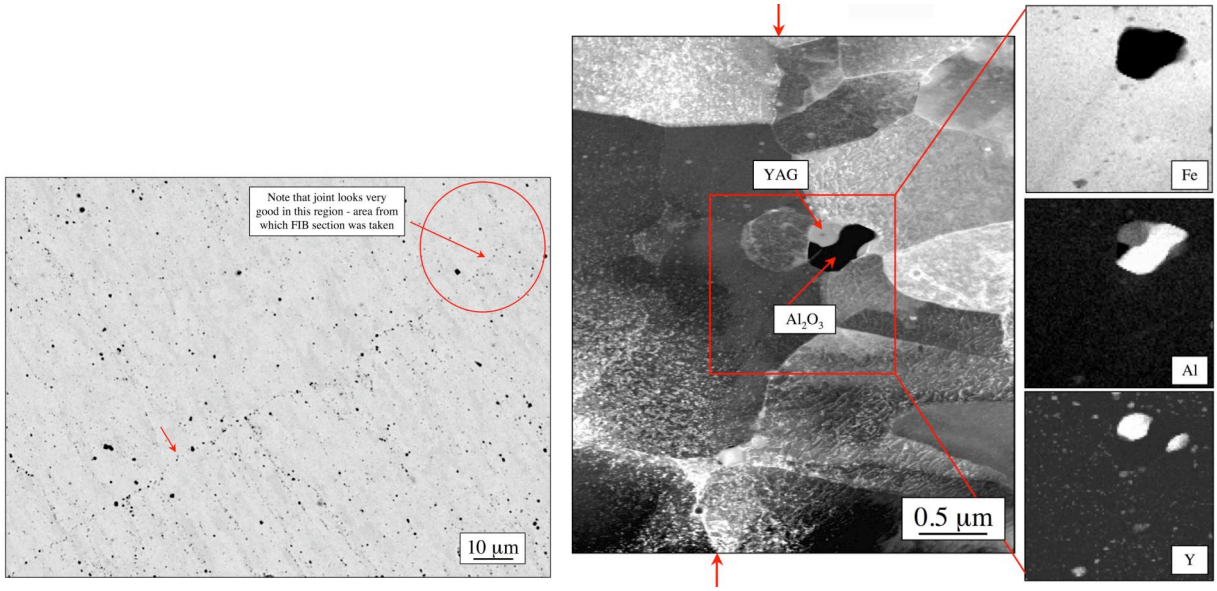

(a) Metallographic cross section

(b) TEM of area indicated in (a), showing the inclusion to be YAG + Al_2O_3

Figure 17. Cross Section of a Joint made by Plasma-Assisted Diffusion Bonding of MA956 to Itself

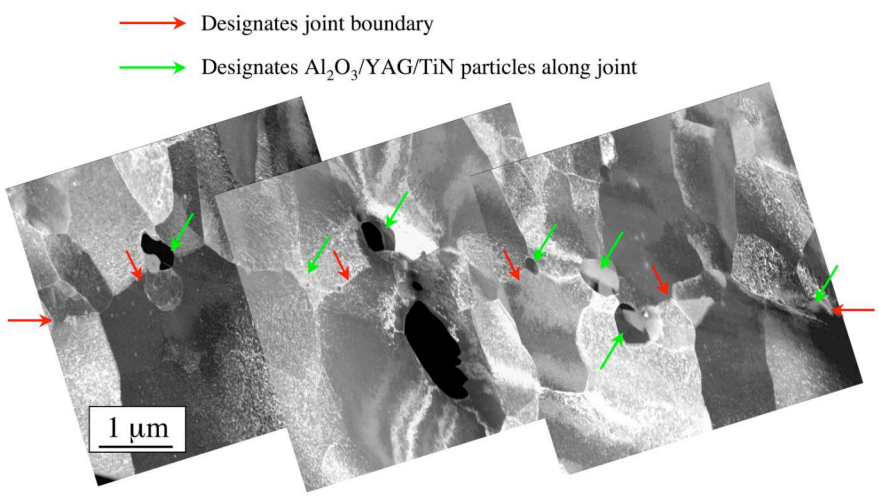

Figure 18. TEM of a Cross Section of the Joint Shown in Fig. 17.

the joints in earlier processing. The compilation of TEM images of part of the joint (Fig. 18) shows it to be extremely clean, except for the discrete particles noted, which were identified as mostly agglomerates of alumina and YAG. The X-ray image for Y showed that, despite these agglomerations, the distribution of Y in the alloy grain boundary and grain boundaries appeared to be largely undisturbed.

OXIDATION-LIMITED LIFETIMES

Because the oxide formed on alumina scale-forming ODS FeCrAl alloys is thin and uniform in thickness, and thickens very slowly with time until almost the end of service life, it is not possible to assess the remaining life of the alloy from measurements of component section thinning. As a result, there is a need for a means of assessing the expected service lifetime based on an understanding of the oxidation behavior of the alloy. The basis for modeling the oxidation-limited lifetimes of these ODS FeCrAl alloys is relatively straight forward [14,15], because of the following:

1. they form essentially pure Al_2O_3 scales that are uniform in thickness;
2. there is negligible internal attack; and
3. the Al concentration gradient in the alloy is considered to be essentially flat until very near the end of life.

Given these assumptions, it is possible simply to equate the oxidation lifetime to the rate of consumption of the available Al to form the alumina scale. That is,

Service life = (Al available for oxidation) / (Al used to form oxide ≡ oxidation rate)

$$= \{[S*10^{-4}*\rho_A*A_\tau*e^{-Q\tau/(1.987*T)}]^2/(3600*A_2*e^{-Q2/(1.987*T)})\} + \{[1/(3600*M)*(V/A)*(\rho_M/(A_3*e^{-Q3/(1.987*T)}))*[(C_{Bo} - C_{Bb}) - M*S*10^{-4}*(A/V)*(\rho_A/\rho_M)*A_\tau*e^{-Q\tau/(1.987*T)}]\} \text{ hours}$$

where:
ρ_A is the density of alumina = 3.97 gcm^{-3} (used in the absence of an actual value for a thermally-grown oxide), and ρ_M = the density of the alloy (= 7.2 gcm^{-3})
A_2 and A_3 are Arrhenius constants for the parabolic and linear oxidation stages, respectively
A_τ is the Arrhenius constant for $\tau_{2\text{-}3}$, the oxide thickness (in μm) at the transition from parabolic to linear oxidation, determined experimentally
Q_2, Q_3, and Q_τ are the activation energies (kcal/mole) for the parabolic and linear oxidation stages, and $\tau_{2\text{-}3}$, respectively
T is the metal temperature (°K)
C_{Bo} = the initial mass fraction of Al in the alloy
C_{Bb} = the mass fraction of Al in the alloy at which a protective Al_2O_3 can no longer form
A = the area exposed to oxidation (cm^2)
V = the volume of alloy being oxidized (cm^3)
S converts mass of Al_2O_3 formed to mass gain of oxygen (= 0.4707)
M converts mass gain of oxygen to mass of Al consumed (= 1.1246)

Figure 19 illustrates a typical mass change-time curve for alloy MA956 oxidized at 1300°C in air until breakaway oxidation occurred, which is taken to indicate the end of useful service life. For the purposes of analysis, the oxidization behavior can be divided into three stages:

Stage 1 is the initial stage when the protective scale is first developed; for most alloys, the oxidation rate in this stage is somewhat faster than that of the fully-established scale, since it typically reflects the formation of a small amount of the oxides of the other elements in the alloy (transient oxides) that can form before the expected steady-state scale becomes continuous. For this alloy class, Stage 1 is sufficiently short that it is neglected.

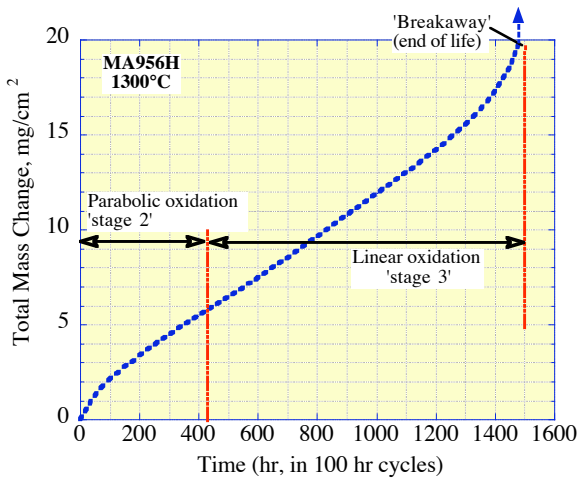

Figure 19. Typical mass change-time curve for alloy MA956HT oxidized at 1300°C in air.

Stage 2, which corresponds to a period of oxidation with essentially no scale spallation, so that the net oxidation rate is controlled by diffusion through the steady-state scale (in this case, alumina) and generally follows a parabolic rate law.

Stage 3, which represents the condition when the scale as a whole continues to thicken, but also a certain amount of scale spallation is occurring, typically from specimen corners. The net result is that the overall oxidation rate follows a different rate law; in this case, observation suggests that oxidation follows an essentially linear rate.

Based on this analysis of the oxidation behavior of the ODS-FeCrAl alloys, a two-stage model currently is used (representing Stages 2 and 3). Thus,

Oxidation lifetime (or time until breakaway occurs), t_b, is given by:

t_b = [length of the parabolic oxidation stage (Stage 2)] + [(Al remaining) / (rate of Al consumed during the linear oxidation stage in Stage 3)].

CALCULATED AND OBSERVED LIFETIMES

Mass-change kinetics are being measured for specimens of the various ODS FeCrAl alloys oxidized at temperatures in the range 1100-1300°C until breakaway oxidation occurs. The end of the protective behavior, i.e., end of service life, is readily recognized by a color change in the oxide scale from white to pink to red-brown, as iron enters the scale as a precursor to breakaway oxidation, and from the oxidation rate curves by the rapid increase in rate of mass gain. From the individual oxidation kinetic curves, the values of the rate constants for Stages 2 and 3 are calculated, as well as the point at which the transition from Stage 2-3 occurred ($\tau_{2\text{-}3}$). From these data, Arrhenius plots are made to obtain the temperature dependence of the individual oxidation rates. In addition, measurement of Al concentration profiles by electron probe micron analysis for these specimens, and for others oxidized for given fractions of their lifetime at each temperature, are used to establish the alumina content in the alloy immediately preceding breakaway. This is the value taken as C_{Bb}. Substitution of these values into the model produces a prediction of the oxidation lifetimes as a function of specimen shape [as defined by *V/A;* note that, for a tube size of 1 in. O.D. x 0.1 in. wall (25.4 x 2.54 mm), the value of *V/A* is 0.64 mm] and temperature; results are shown in Fig. 20. Also superimposed in Fig. 20 are actual experimentally-measured oxidation

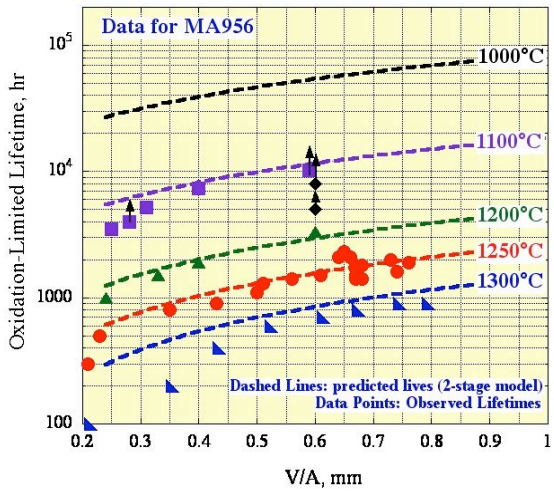

Figure 20. Comparison of observed and calculated oxidation-limited lifetime of MA956 oxidized at 1000-1300°C in air.

lifetimes at various temperatures. It can be seen that there is good agreement between observed and calculated values of t_b, but there is a tendency to over-predict the oxidation life at the smaller *V/A* values.

Figure 21 compares the lifetimes at 1100°C predicted for all of the alloys considered, as a function of *V/A*. Of note is the fact that, while the lifetimes for alloys MA956H, PM2000, ODM751, ODS-Fe_3Al, are reasonably similar (with PM2000 showing the longest lifetime), alloy MA956 exhibits significantly shorter lifetimes, for reasons that are not well understood.

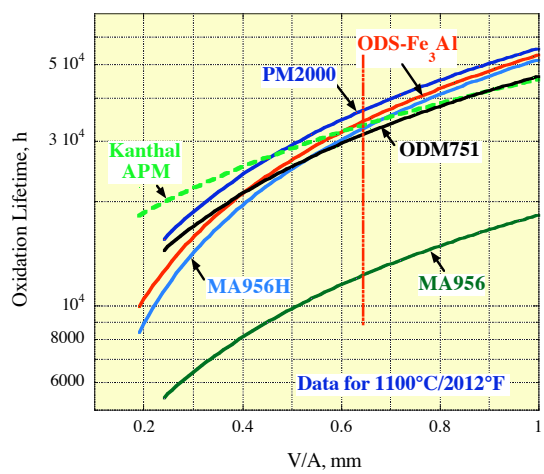

Figure 21. Predicted oxidation-limited service lifetimes kinetics for several ODS-FeCrAl alloys (the vertical line indicates the value of *V/A* for a tube 25.4 mm diam x 2.54 mm wall).

SUMMARY

Overall, the early goal of the program—to develop an ODS-version of the ORNL Fe_3Al with mechanical properties (creep strength) comparable to current commercial ODS-FeCrAl alloys, while retaining the exceptional oxidation and sulfidation resistance of iron aluminide—has been achieved. The main focus of

the project is now to address the major issues that limit the acceptance for use of this general class of ODS alloys, which are (1) difficulty in joining; (2) significantly lower mechanical properties normal to the extrusion direction; and (3) difficulty in assessing service lifetime. Progress has been made in demonstrating that the alloys can be joined by techniques other than fusion welding, and emphasis has been placed on quantifying the creep strength of such joints, and to understanding the implications of the associated microstructural modifications. Routes have been explored for improving the transverse strength (hoop strength in tubes), and modification of the post-extrusion processing to promote the development of a spiral grain structure upon recrystallization is the focus of current activity. This route has been shown to be capable of producing the intended influence on the recrystallization behavior, but better control is needed. A simple model relating service life to aluminum consumption during high-temperature oxidation provides reasonable agreement with observed oxidation-limited lifetimes in laboratory exposures in air. Continuing studies are measuring the critical parameters used by the model and their temperature dependence, as well as defining the influence of specimen shape (to ensure that the model is applicable to tubes, and is not unduly influenced by the geometry of the laboratory coupons used to develop its parameters).

ACKNOWLEDGEMENTS

The research was sponsored by the Fossil Energy Advanced Research Materials Program, Office of Fossil Energy, U. S. Department of Energy under contract DE-AC05-00OR22725 with UT-Battelle, LLC. We are indebted to our co-workers: Hu Longmire, who was responsible for preparing the metallographic cross sections; Larry Walker for the electron-probe microanalysis examinations; and to Karren More who performed the TEM analyses.

REFERENCES

1. F. Starr and I.A. Shibli, "Fundamental Issues in the development of Austenitic and Nickel-Based Alloys for Advanced, Supercritical Steam and High-Temperature Indirect-Fired Gas Turbine Systems, " pp. 459-471 in Proc. 5th Intl. Charles Parsons Turbine Conference, Eds:. A. Strang, W.M. Banks, R.D. Conroy, G.M. McColvin, J.C. Neal, and S. Simpson, IOM Communications Ltd. (2000).
2. P.F. Tortorelli, J.H. DeVan, B.A. Pint, and I.G. Wright, "High-Temperature Corrosion Behavior of Iron-Aluminide Alloys and Coatings," paper presented at the 9th Annual Conference on Fossil Materials, Oak Ridge, Tennessee, May 1995.
3. B. Kad, J. Heatherington, I. G. Wright, and V. K. Sikka, "Optimization of ODS FeCrAl and Fe_3Al properties," Proc. 17th Ann. Conf. on Fossil Energy Materials," Baltimore, Maryland, April 2003.
4. D.M. Jaeger and A.R. Jones, "The Development of Grain Shape in Iron-Based ODS Alloys," pp. 1515-1522 in Materials for Advanced Power Engineering 1994, Part II, Eds: D. Coutsouradis, J.H. Davidson, J. Ewald, P. Greenfield, T. Khan, M. Malik, D.B. Meadowcroft, V. Regis, R.B. Scarlin, F. Schubert, and D.V. Thornton, Kluwer Academic Publishers (1994).
5. P.L. Threadgill, Friction Welding of an Fe_3Al-based ODS Alloy, Report No. ORNL/Sub/97-SX373/01, July 1998. See, also, B. J. Inkson and P. L. Threadgill, "Friction Welding of Fe-40Al Grade 3 ODS Alloy," *Mat. Sci. and Eng.*, A258, 313-318 (1998).
6. B. Kad, "Optimization of Oxide Dispersion-Strengthened Alloy Tubes," Proc. 19th Annual Conference on Fossil Energy Materials, Knoxville, Tennessee May 9-11, 2005, https://www.ms.ornl.gov/FEM19

7. D.J. Seery and J. Sangiovanni, "Engineering development of a coal-fired high-performance power generating system," Paper No. 1.7 in Proc. of the Advanced Coal-Based Power and Environmental Systems'98 Conference, Morgantown, West Virginia, July 21-23, 1998, DOE/FETC-98/1072.
8. S. Holmstrom, M. Siren, L. Heikinheimo, P. Auerkari, J. Varmavuo, and R. Saarinen, "Performance of an Iron-Based ODS Alloy in a Boiler Environment," pp. 769-777 in Materials for Advanced Power Engineering 1998, J. LeCompte-Beckers, F. Schubert, and P. J. Ennis, Eds., Forschungszentrum Juelich Zentralbibliothek, Germany (1998).
9. F. Starr, A. R. White, and B. Kazimierzak, in Materials for Advanced Power Engineering 1994, D. Coutsouradis, et al., Eds., (Kluwer Academic Publishers, 1994) pp. 1393-1412.
10. M.L. Hamilton, et al., "Fabrication Technological Development of the Oxide Dispersion-Strengthened Alloy MA957 for Fast Reactor Applications," Report No. PNNL-13168, on work under US DOE Contract No. DE-AC06-76RLO 1830, Feb, 2000.
11. B. Kad, "Optimization of Oxide Dispersion-Strengthened Alloy Tubes," Proc. 19th Annual Conference on Fossil Energy Materials, Knoxville, Tennessee May 9-11, 2005, https://www.ms.ornl.gov/FEM19
12. J.P. Hurley, K.D. Williams, G.F. Weber, and M.L. Jones, "Very High-Temperature ODS Alloy Heat Exchangers for Solid-Fuel Thermal Systems," Paper presented at the 27th Intl. Technical Conf. on Coal Utilization and Fuel Systems, Clearwater, Florida (2002).
13. P. Muangjunburee and G.J. Tatlock, "The Study of α-alumina Scale Failure at Welded Joints in High-Temperature ODS Alloys," Proc. Intl. Symp: "Corrosion Science in the 21st Century," University of Manchester Institute of Science and Technology, Manchester, England, 6-11 July, 2003.
14. W. J. Quadakkers and K. Bongartz, Werkstoffe und Korrosion, 45, 232-41 (1994).
15. M. J. Bennett, H. Romary and J. B. Price, "The Oxidation Behavior of Alumina-Forming Oxide Dispersion-Strengthened Ferritic Alloys at 1200-1400°C," pp. 95-103 in Heat Resistant Materials, K. Natesan and D. J. Tillack, eds. (ASM, Materials Park, Ohio, 1991).